Geophysical Prospecting

EAGE EUROPEAN ASSOCIATION OF GEOSCIENTISTS & ENGINEERS

Geophysical Prospecting doi: 10.1111/1365-2478.12097

Three-dimensional inversion of towed streamer electromagnetic data

Michael S. Zhdanov[1,2]*, Masashi Endo[1], Leif H. Cox[1], Martin Čuma[1,3], Johnathan Linfoot[4], Chris Anderson[5], Noel Black[1] and Alexander V. Gribenko[1,2]

[1]*TechnoImaging, 4001 South, 700 East, Suite 500, Salt Lake City, Utah 84107, USA,* [2]*Department of Geology and Geophysics, University of Utah, 115 South, 1460 East, Room 383, Salt Lake City, Utah 84112, USA,* [3]*Center for High Performance Computing, University of Utah, 155 South, 1452 East, Room 405, Salt Lake City, Utah 84112, USA,* [4]*Petroleum GeoServices, Birch House, 10 Bankhead Crossway South, Edinburgh EH11 4EP, UK, and* [5]*Petroleum GeoServices, 4 The Heights, Brooklands, Weybridge, Surrey KT13 0NY, UK*

Received January 2012, revision accepted May 2013

ABSTRACT

A towed streamer electromagnetic system capable of simultaneous seismic and electromagnetic data acquisition has recently been developed and tested in the North Sea. We introduce a 3D inversion methodology for towed streamer electromagnetic data that includes a moving sensitivity domain. Our implementation is based on the 3D integral equation method for computing responses and Fréchet derivatives and uses the re-weighted regularized conjugate gradient method for minimizing the objective functional with focusing regularization. We present two model studies relevant to hydrocarbon exploration in the North Sea. First, we demonstrate the ability of a towed electromagnetic system to detect and characterize the Harding field, a medium-sized North Sea hydrocarbon target. We compare our 3D inversion of towed streamer electromagnetic data with 3D inversion of conventional marine controlled-source electromagnetic data and observe few differences between the recovered models. Second, we demonstrate the ability of a towed streamer electromagnetic system to detect and characterize the Peon discovery, which is representative of an infrastructure-led shallow gas play in the North Sea. We also present an actual case study for the 3D inversion of towed streamer electromagnetic data from the Troll field in the North Sea and demonstrate our ability to image all the Troll West Oil and Gas Provinces and the Troll East Gas Province. We conclude that 3D inversion of data from the current generation of towed streamer electromagnetic systems can adequately recover hydrocarbon-bearing formations to depths of approximately 2 km. We note that by obviating the need for ocean-bottom receivers, the towed streamer electromagnetic system enables electromagnetic data to be acquired over very large areas in frontier and mature basins for higher acquisition rates and relatively lower cost than conventional marine controlled-source electromagnetic methods.

Key words: Electromagnetic, Sensitivity domain, Modelling.

1 INTRODUCTION

The premise of the various marine controlled-source electromagnetic (MCSEM) methods is sensitivity to the lateral extents and thicknesses of resistive bodies embedded in conductive hosts. Over the past decade, MCSEM surveys characterized by arrays of fixed ocean-bottom receivers and towed transmitters have been applied to de-risking exploration and appraisal projects with direct hydrocarbon indication (e.g., Constable 2012). The most successful applications of MCSEM to date have been in complement to those seismic interpretations where lithological or fluid variations cannot be

*Corresponding author. Email: mzhdanov@technoimaging.com.

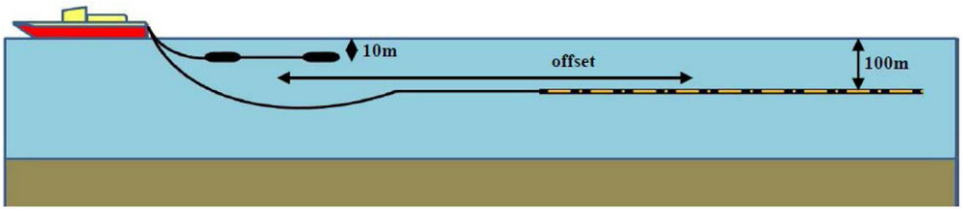

Figure 1 A schematic representation of a towed streamer EM system with a single transmitter in a streamer towed 10 m below the sea-surface and multi-offset receivers in a streamer nominally towed 100 m below the sea-surface.

adequately discriminated by seismic methods alone (e.g., Hesthammer *et al.* 2010). However, relatively high acquisition costs have represented a significant obstacle to widespread adoption of conventional MCSEM technology. To this end, a towed streamer system capable of simultaneous seismic and electromagnetic (EM) data acquisition has recently been developed and tested in the North Sea (Anderson and Mattsson 2010; Mattsson *et al.* 2010; Linfoot *et al.* 2011; McKay *et al.* 2011) (Fig. 1). We note that, independently, a short-offset towed EM system has been developed and tested for gas hydrate mapping in the Gulf of Mexico (Weitemeyer and Constable 2011). The moving platform geometry of a towed EM system enables EM data to be acquired over very large areas in both frontier and mature basins for higher acquisition rates and lower costs compared to conventional MCSEM methods.

Hydrocarbon reserves and resources are estimated with varying confidence from volumetrics predicted from different subsurface models and scenarios. As such, acquisition, data processing and quality control measures represent just part of a successful exploration workflow. Quantitative interpretation of EM data is inherently reliant upon 3D earth models derived from inversion since EM data cannot simply be separated or transformed with linear operators as per seismic methods. However, methods for inverting EM data are complicated by the very small, non-unique and non-linear responses of the hydrocarbon-bearing reservoir units when compared to the measured total fields. Moreover, 3D inversion of towed streamer EM data poses a significant challenge because of the size of the surveys, the requirement for high resolution models and the significantly increased number of transmitter-receiver pairs relative to conventional MCSEM surveys.

The primary problem with 3D modelling of towed streamer EM data is the necessity to solve as many linear systems of equations as there are transmitter positions in the survey. In the case of 3D inversion, this problem is exacerbated by the need to compute Fréchet derivatives and repeat the whole process for multiple iterations. Similar to airborne EM (Cox and Zhdanov 2007; Cox, Wilson and Zhdanov 2010, 2012), we can exploit the fact that the towed

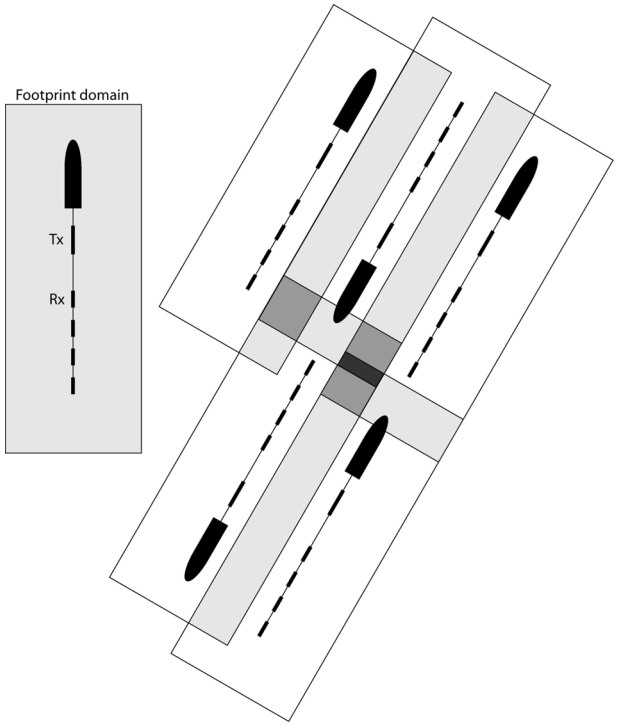

Figure 2 Plan view of multiple towed streamer EM sensitivity domains superimposed over the same 3D earth model. Darker shading indicates a higher fold of different sensitivity domains.

streamer EM system's sensitivity domain is significantly less than the size of the survey area and we introduce the concept of 3D inversion with a moving sensitivity domain. That is, for a given transmitter-receiver pair, the responses and Fréchet derivatives are computed from a 3D earth model that encapsulates the towed EM system's sensitivity. The Fréchet matrix for the entire 3D earth model is then constructed as the superposition of Fréchet derivatives from all transmitter-receiver pairs over the entire 3D earth model (Fig. 2). It follows that memory and computational requirements can be reduced by several orders of magnitude, making large-scale 3D inversion of towed steamer EM data a tractable problem with high-end workstations or moderate cluster resources.

2 INVERSION METHODOLOGY

2.1 Modelling

For completion, we review the basis of 3D EM modelling. Starting from Maxwell's equations, Ohm's law, the usual constitutive relations and assuming an $\exp(-i\omega t)$ time dependence, one can derive inhomogeneous telegrapher's equations for electric fields:

$$\nabla \times \nabla \times \mathbf{E}(\mathbf{r}) - i\omega\mu\sigma(\mathbf{r})\mathbf{E}(\mathbf{r}) = i\omega\mu\mathbf{J}(\mathbf{r}), \tag{1}$$

where $\mathbf{J}(\mathbf{r})$ is the extraneous electric current due to the transmitter. For marine EM systems, the transmitter is best represented as a finite-length electric bipole of arbitrary orientation. In general, the 3D conductivity distribution $\sigma(\mathbf{r})$ can be both frequency-dependent and anisotropic. In order to remove discretization problems associated with discrete sources, the external source terms are replaced with an equivalent distributed background electric field obtained by solving for an earth model excited by the external sources. Explicitly, the conductivity is separated into background $\sigma_b(z)$ and anomalous $\sigma_a(\mathbf{r})$ parts:

$$\sigma(\mathbf{r}) = \sigma_b(z) + \sigma_a(\mathbf{r}) \tag{2}$$

and the background (b) electric fields can be computed from:

$$\nabla \times \nabla \times \mathbf{E}^b(\mathbf{r}) - i\omega\mu\sigma_b(z)\mathbf{E}^b(\mathbf{r}) = i\omega\mu\mathbf{J}(\mathbf{r}). \tag{3}$$

The anomalous (a) electric fields are defined as the difference between the total and background electric fields, respectively, or:

$$\mathbf{E}^a(\mathbf{r}) = \mathbf{E}(\mathbf{r}) - \mathbf{E}^b(\mathbf{r}). \tag{4}$$

We obtain the inhomogeneous telegrapher's equation for the anomalous electric field by subtracting equation (3) from equation (1):

$$\nabla \times \nabla \times \mathbf{E}^a(\mathbf{r}) - i\omega\mu\sigma(\mathbf{r})\mathbf{E}^a(\mathbf{r}) = i\omega\mu\sigma_a(\mathbf{r})\mathbf{E}^b(\mathbf{r}). \tag{5}$$

The background electric fields can be computed semi-analytically from equation (3) as Hankel transforms of elementary functions. Equation (5) avoids errors associated with the discretization of the external source terms. This approach has been widely used in the EM modelling literature, whether with finite-difference (FD) (e.g., Mackie, Watts and Rodi 2007; Commer and Newman 2008), finite-volume (FV) (e.g., Weiss and Constable 2006), finite-element (FE) (e.g., da Silva *et al.* 2012), or integral equation (IE) methods (e.g., Hursán and Zhdanov 2002; Zhdanov 2002, 2009). The advantage of the volume IE method over the other numerical methods is that the entire 3D earth model need not be discretized. Rather, an appropriate background conductivity model is chosen and the volume of interest is discretized with all boundary conditions perfectly matched. This is unlike FD, FV or FE methods that require large-scale discretization and an appropriate choice of boundary conditions so as to emulate an unbound 3D earth model. Later, we shall discuss how the dimensions of that volume of interest (or sensitivity domain) are chosen.

From equation (5), it is well-known that we can derive a vector Fredholm integral equation of the second kind for anomalous electric fields:

$$\mathbf{E}^a(\mathbf{r}') = \int\int\int_V \widehat{\mathbf{G}}_E(\mathbf{r}', \mathbf{r}) \cdot \sigma_a(\mathbf{r}) \left[\mathbf{E}^b(\mathbf{r}) + \mathbf{E}^a(\mathbf{r})\right] dv, \mathbf{r}' \subset V, \tag{6}$$

where $\widehat{\mathbf{G}}_E(\mathbf{r}', \mathbf{r})$ is the body-to-body electric Green's tensor for the background conductivity model (e.g., Raiche 1974; Hohmann 1975; Weidelt 1975; Xiong 1992). The integration is evaluated over those volumes of interest where the conductivity differs from the background conductivity. This means that we can simultaneously solve equation (6) for multiple (D) domains (Endo, Cuma and Zhdanov 2009):

$$\mathbf{E}^a(\mathbf{r}') = \sum_{i=1}^{N} \int\int\int_{V_i} \widehat{\mathbf{G}}_E(\mathbf{r}', \mathbf{r}) \cdot \sigma_a(\mathbf{r}) \left[\mathbf{E}^b(\mathbf{r}) + \mathbf{E}^a(\mathbf{r})\right] dv. \tag{7}$$

Each of the domains may be of different dimensions and discretizations. For example, we may finely discretize one domain for bathymetry, have another coarsely discretized for regional (background) structures and finely discretize another domain incorporating those formations of interest. All of these domains are fully coupled through equation (7). Using the method of moments, equation (7) can be reduced to the linear system:

$$(\mathbf{I} - \mathbf{\Gamma} \cdot \boldsymbol{\sigma}_a) \cdot \mathbf{E}^a = \mathbf{\Gamma} \cdot \boldsymbol{\sigma}_a \cdot \mathbf{E}^b, \tag{8}$$

where $\mathbf{E}^a$ is the vector of the anomalous electric fields, $\mathbf{I}$ is the identity matrix, $\mathbf{\Gamma}$ is the matrix of volume-integrated body-to-body electric Green's tensors for the background conductivity model and $\boldsymbol{\sigma}_a$ is a diagonal matrix of anomalous conductivities. Note that equation (7) requires the total electric field in each cell and this is computed as the sum of the background and anomalous electric fields. This summation propagates numerical errors due to finite precision. By adding the background electric fields to both sides of equation (8) and after some algebra, we can instead obtain the linear system:

$$(\mathbf{I} - \mathbf{\Gamma} \cdot \boldsymbol{\sigma}_a) \cdot \mathbf{E} = \mathbf{E}^b, \tag{9}$$

which directly solves for the 'total' electric field, **E**, instead of the anomalous electric field, $\mathbf{E}^a$, while retaining the distributed source in terms of the background electric fields, $\mathbf{E}^b$. This is a unique property of integral equation methods and their hybrids. That said, equation (9) requires the solution of a large, dense and ill-conditioned matrix system. Following Singer and Fainberg (1995) and Hursán and Zhdanov (2002), we pre-condition equation (9) with contraction operators to improve the conditioning of the matrix system. Also as per Hursan and Zhdanov (2002) and Avdeev *et al.* (1997), we exploit the Toeplitz structure of matrix system (9), meaning that we can perform multiplications of the translationally invariant horizontal components of $\mathbf{\Gamma}$ without needing to store its full size. We solve equation (9) using the complex generalized minimum-residual method (CGMRES), as this has been proven to always converge (Zhdanov 2002). With equidistance x and y discretizations in each of the domains, matrix-vector multiplications in the CGMRES solution of matrix equation (9) can be provided by 2D FFT convolutions that reduce computational complexity from $O(n^2)$ to $O(n \log n)$. This method restricts the discretization in each domain to be uniform in the horizontal directions but arbitrary in the vertical directions.

Following the solution of equation (9), the electric fields at the receivers are computed from the following expression:

$$\mathbf{E}\left(\mathbf{r}'\right) = \mathbf{E}^b\left(\mathbf{r}'\right) + \int\int\int_V \widehat{\mathbf{G}}_E\left(\mathbf{r}', \mathbf{r}\right) \cdot \sigma_a\left(\mathbf{r}\right) \mathbf{E}\left(\mathbf{r}\right) dv, \tag{10}$$

where $\widehat{\mathbf{G}}_E\left(\mathbf{r}', \mathbf{r}\right)$ is now the body-to-receiver electric Green's tensor for the background conductivity model.

Zhdanov *et al.* (2011) discussed iterative migration for explicitly evaluating the direction of steepest descent required for deterministic inversion methods. Given the typically low conductivity contrasts (e.g., < 100:1) of sedimentary and reservoir formations, our numerical analyses comparing iterative migration and linearized inversion have demonstrated that the Fréchet derivatives can be computed accurately and rapidly using the quasi-Born approximation:

$$\frac{\partial \mathbf{E}\left(\mathbf{r}'\right)}{\partial \sigma_k} = \int\int\int_{V_k} \widehat{\mathbf{G}}_E\left(\mathbf{r}', \mathbf{r}\right) \cdot \mathbf{E}\left(\mathbf{r}\right) dv. \tag{11}$$

This method is more accurate than the Born approximation (e.g., Gribenko and Zhdanov 2007; Støren, Zach and Maaø 2008) and it explicitly avoids additional modelling as required by formally invoking the reciprocity theorem (e.g., McGillivray *et al.* 1994).

2.2 Inversion

The modelling of towed streamer EM data can be expressed in operator form as follows:

$$\mathbf{d} = A(\mathbf{m}), \tag{12}$$

where $\mathbf{d}$ is the N_d length vector of observed data, $\mathbf{m}$ is the N_m length vector of conductivities and A is the non-linear modelling operator. Towed streamer EM data are finite in their spatial and frequency content and are contaminated with noise. This means their inversion is ill-posed because they are inherently non-unique and unstable and regularization must be introduced to obtain a unique and stable solution (Tikhonov and Arsenin 1977). Regularization is a broad term that includes the interpreter's prejudice toward model dimensionality, constraints and model class. All geological constraints manifest themselves through regularization, such as data weights, model upper and lower bounds, model weights, *a priori* model and the type of stabilizing functional. We can solve equation (12) using the Tikhonov parametric functional with a pseudo-quadratic stabilizer (Zhdanov 2002):

$$P^\alpha(\mathbf{m}, \mathbf{d}) = \varphi\left(\mathbf{m}, \mathbf{d}\right) + \alpha s\left(\mathbf{m}\right) \rightarrow \min, \tag{13}$$

where $\varphi\left(\mathbf{m}, \mathbf{d}\right)$ is a misfit functional:

$$\varphi\left(\mathbf{m}, \mathbf{d}\right) = \left(\mathbf{W}_d A(\mathbf{m}) - \mathbf{W}_d \mathbf{d}\right)^T \left(\mathbf{W}_d A(\mathbf{m}) - \mathbf{W}_d \mathbf{d}\right) \tag{14}$$

and $s\left(\mathbf{m}\right)$ is a pseudo-quadratic stabilizer:

$$s\left(\mathbf{m}\right) = \left(\mathbf{W}_e \mathbf{W}_m \mathbf{m} - \mathbf{W}_e \mathbf{W}_m \mathbf{m}_{apr}\right)^T \left(\mathbf{W}_e \mathbf{W}_m \mathbf{m} - \mathbf{W}_e \mathbf{W}_m \mathbf{m}_{apr}\right). \tag{15}$$

In equation (15), $\mathbf{W}_d$ and $\mathbf{W}_m$ are the diagonal data and model weighting matrices, respectively; $\mathbf{W}_e$ is a diagonal matrix used to select a type of stabilizing functional; α is a regularization parameter that balances (or biases) the misfit and stabilizing functionals. We perform our inversion in the space of logarithmic model parameters (log conductivity) and logarithmic data so as to reduce the dynamic range of both the model parameters and the data. This improves numerical stability through an improved conditioning of the Fré chet matrix. As discussed by Zhdanov *et al.* (2011), there are a variety of stabilizing functionals to choose from and these are chosen with the user's prejudice for the expected geology. Rather than using smooth stabilizing functionals, our preference is to use focusing stabilizing functionals that recover models with sharp resistivity contrasts (Portniaguine and Zhdanov 1999). In all results presented in this paper, we have used the minimum vertical support (MVS) stabilizer (Zhdanov, Gribenko

and Cuma 2008), which has the following expression for the matrix $\mathbf{W}_e$:

$$\mathbf{W}_e^{MVS} = \mathbf{diag}\left[\frac{1}{\left(\int_S m^2 ds + e^2\right)^{1/2}}\right], \quad (16)$$

where e is a small number (focusing parameter) introduced to avoid singularity when $\mathbf{m} = \mathbf{m}_{apr}$ and where S is a horizontal section from the inversion domain. The MVS stabilizer minimizes the thickness of the volume with non-zero departures from the *a priori* model and was specifically developed to invert for thin sub-horizontal structures typical of reservoir formations. Equation (13) can be solved using a variety of optimization methods. We minimize equation (13) using the re-weighted regularized conjugate gradient (RRCG) method and refer the reader to Zhdanov (2002) for further details of this method.

2.3 Moving sensitivity domains

Conventional MCSEM surveys may have in the order of hundreds of fixed receivers and in the order of thousands of transmitter positions. Reciprocity is routinely exploited in 3D MCSEM modelling and inversion to minimize the number of source terms that need to be solved (e.g., Zhdanov *et al.* 2011). At the same time, towed streamer EM surveys may have thousands of transmitter positions and thousands of receiver positions. Therefore, reciprocity cannot be exploited for any computational efficiency. In this respect, towed streamer EM surveys are similar to airborne EM (AEM) surveys for which, until recently, 3D inversion was considered intractable. It had long been known that a particular transmitter-receiver pair were sensitive only to a limited volume of earth called the 'footprint' (e.g., Liu and Becker 1990; Beamish 2003; Reid, Pfaffling and Vrbancich 2006), which we hereafter refer to as a 'sensitivity domain', which contains the majority (e.g., > 90%) of the integrated sensitivity of the particular transmitter-receiver pair. Exploiting the fact that this sensitivity domain is significantly smaller than the area of a survey, *Cox et al.* (2010, 2012) computed the responses and Fréchet derivatives only for that part of the 3D earth model that is within the EM system's sensitivity domain and then superimposed the Fré chet derivatives for all sensitivity domains into a single, sparse Fré chet matrix for the entire 3D earth model. This reduced the memory and computational requirements by several orders of magnitude. For example, the number of non-zero elements in each row of the Fréchet matrix is just the number of cells within each sensitivity domain (in the order of thousands) rather than the total number of cells in the model (in the order of millions). This has made it practical to invert AEM data from hundreds of thousands of transmitter positions to megacell 3D earth models. Čuma, Wilson and Zhdanov (2012) recently extended this concept to potential fields and discussed selection criteria for the sensitivity domain size.

We use a similar moving sensitivity domain concept for the inversion of towed streamer EM data. The responses and Fréchet derivatives of the towed streamer EM system can be calculated from the spatially finite sensitivity domain without any appreciable loss of accuracy. The dimensions of the sensitivity domain are dependent on the transmitter and/or receiver locations, geometries and components of the observed data, spectral content of the data and subsurface physical properties and are much smaller than the volume of the entire earth model. To illustrate this concept, Fig. 2 shows a plan view of multiple towed streamer EM sensitivity domains superimposed over the same 3D earth model. Darker shading indicates a higher fold of different sensitivity domains. As an example of the size of the sensitivity domain (corresponding to the Peon model study presented later in this paper), we can calculate the integrated sensitivities for a towed streamer EM system consisting in a 300 m long electric bipole transmitter towed 10 m below the sea-surface and in-line electric field receivers towed 100 m below the sea-surface at offsets between 1325–2545 m at 0.10 and 1.00 Hz. While the actual system may have intermediate offsets and other frequencies, these are representative of both the highest frequency/shortest offset and the lowest frequency/longest offset configurations. The earth model consisted in a 384 m thick 0.3 ohm-m water column overlying an otherwise homogeneous, isotropic half-space of 3.0 ohm-m. Since the isosurfaces of the integrated sensitivities are the functions of transmitter-receiver geometry, frequency and earth model, it is convenient (from a programming perspective) to encapsulate them in a rectangular domain. For example, as can be seen in Fig. 3, a sensitivity domain of dimension 8 km x 5 km x 1.5 km captures over 95% of the integrated sensitivity for the towed streamer EM system for all frequencies and offsets. Note that this sensitivity domain is significantly smaller than the size of the actual Peon earth model presented later in this paper. Moreover, we note that the sensitivity domain dimensions do not need to be constant and can vary as a function of offset and frequency.

The Fréchet derivatives (sensitivities) of the EM data for the entire towed streamer EM survey and entire subsurface model can be constructed as the superposition of the Fréchet derivatives from all of the sensitivity domains determined for the corresponding positions of the towed streamer EM system. The Fréchet matrix for the entire sea-bottom model is

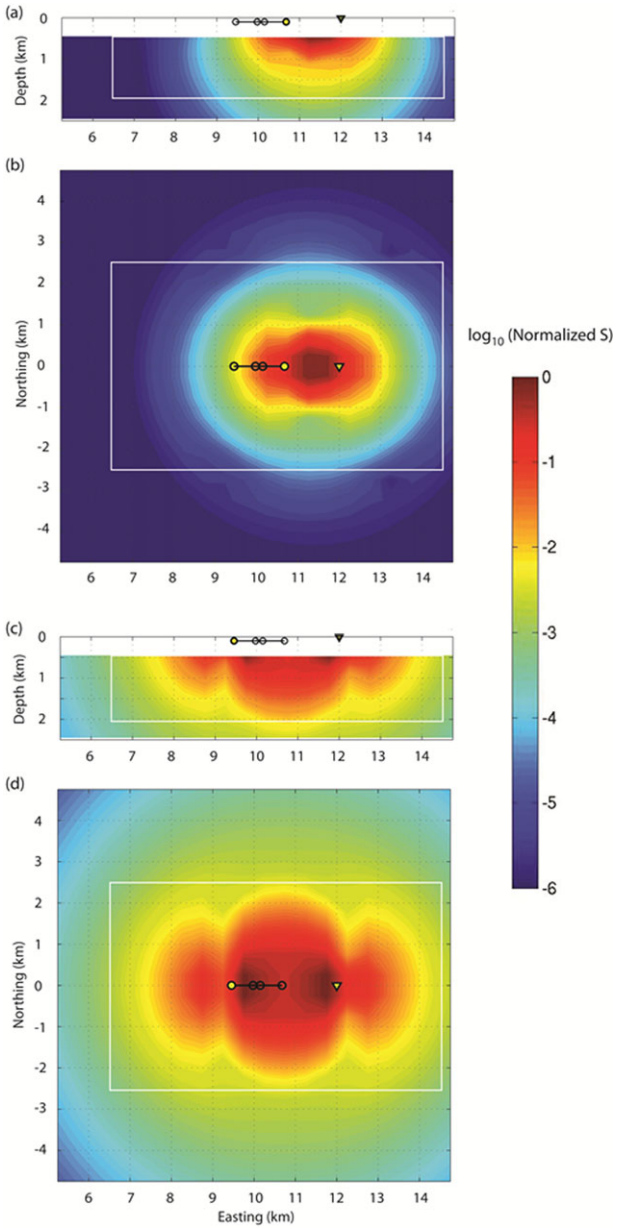

Figure 3 Example of the vertical (panels a and c) and horizontal (panels b and d) dimensions of a sensitivity domain used in the Peon model study. This figure presents the integrated sensitivities for a towed streamer EM system consisting in a 300 m long electric bipole transmitter towed 10 m below the sea-surface and in-line electric field receivers towed 100 m below the sea-surface at offsets between 1325 m for 1.00 Hz (panels a and b) and 2545 m for 0.10 Hz (panels c and d). The earth model consisted in a 384 m thick 0.3 ohm-m water column overlying an otherwise homogeneous, isotropic half-space of 3.0 ohm-m. A sensitivity domain of dimension 8 km x 5 km x 1.5 km (white box) captures over 95% of the integrated sensitivity for the towed streamer EM system for all frequencies and offsets.

calculated and stored as a sparse matrix, rather than a full matrix as per the conventional 3D inversion methods (e.g., Zhdanov 2002, 2009). We also note that there are particular computational advantanges to using the aforementioned IE-based modelling with a moving sensitivity domain. First, the background fields and Green's tensors need not be evaluated beyond the sensitivity domain. Second, the body-to-body electric Green's tensors can be computed for a single sensitivity domain and then translated across the 3D earth model. Third, linear system (9) can be rapidly constructed and solved for the total electric field inside each sensitivity domain and the corresponding electric fields at the receivers and their sensitivities rapidly computed from equations (10) and (11), respectively.

3 MODEL STUDIES

In the following section, we present two model studies that investigate the performance of the 3D inversion of towed streamer EM data. From the analysis of field trial data acquired at several knots, we note that the noise characteristics of the towed streamer EM system are comparable to conventional MCSEM when data are normalized by antenna moments. Detailed analysis of the data acquired during the North Sea field trials concluded that the total electric field noise levels were functions of frequency and offset and are generally below 3% and below 2% between 0.1–1.0 Hz (Mattsson *et al.* 2012). This noise is composed of contributions from measurement system error, navigation error, processing error and electromagnetic noise. It follows that a simple noise model of 2–3% random Gaussian noise is sufficient to emulate the noise characteristics of a towed streamer EM survey. This has been independently observed for mapping gas hydrates in the Gulf of Mexico by Weitemeyer and Constable (2010) with the Vulcan towed EM system developed by the Scripps Institution of Oceanography.

In both model studies to be presented, we used the aforementioned regularized inversion, which is robust with respect to noise. For both model studies, this was tested by adding random 2% Gaussian noise to the 'total' electric fields for the synthetic towed streamer EM data. In both cases, the inversions were run until the normalized misfit calculated as the L2 norm of the residuals divided by the L2 norm of the observed data reached 2%.

3.1 Harding

First, we consider a model study comparing towed streamer EM with conventional MCSEM. Harding is a medium-sized

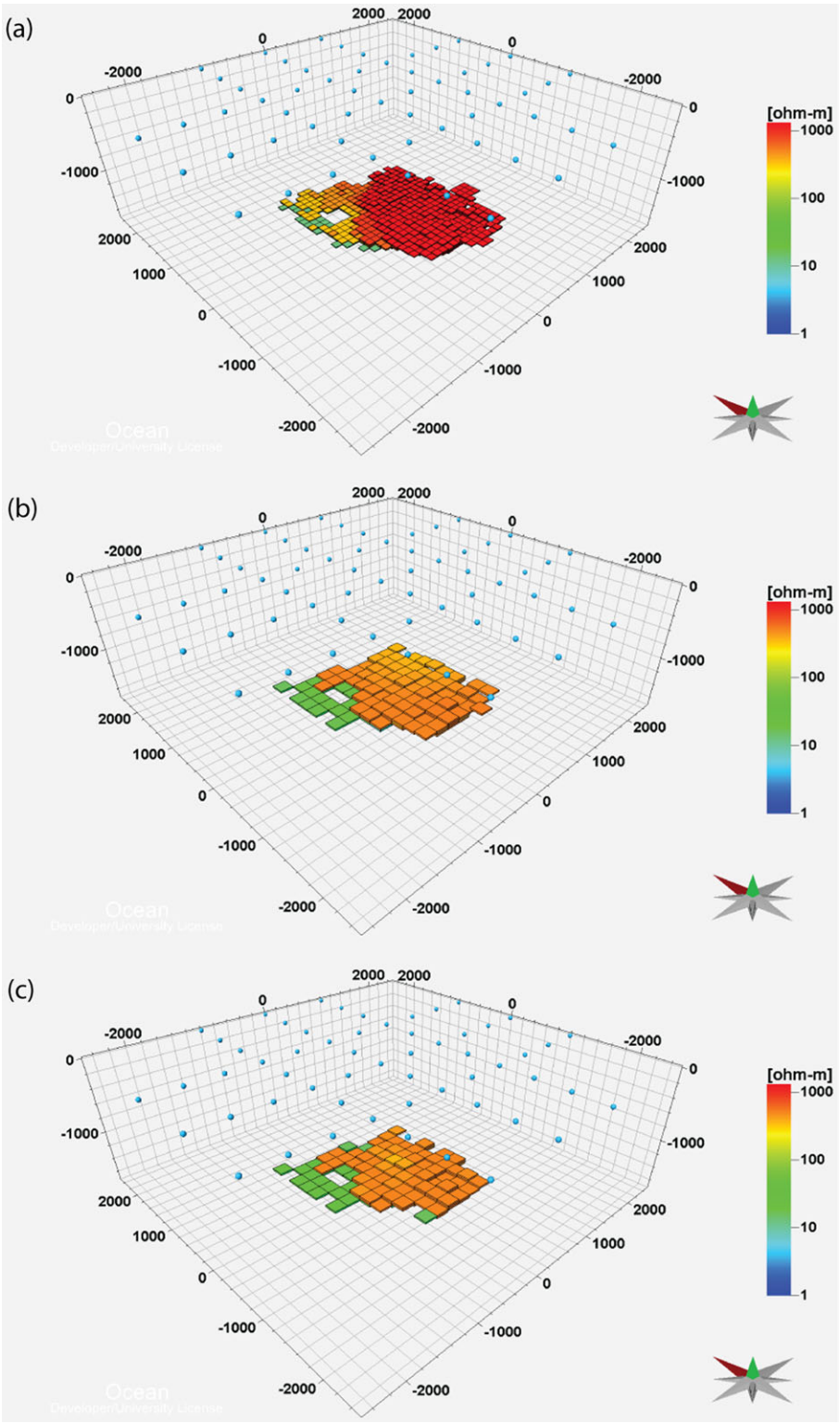

Figure 4 (a) 3D perspective view of the Harding Central reservoir model, with resistivity values greater than 10 ohm-m shown. (b) 3D perspective view of the Harding Central reservoir model recovered from 3D inversion of towed streamer EM data, with resistivity values greater than 10 ohm-m shown. The blue dots indicate the different transmitter positions. (c) 3D perspective view of the Harding Central reservoir model recovered from 3D inversion of conventional marine CSEM data, with resistivity values greater than 10 ohm-m shown. The blue dots indicate the different seefloor-based receiver positions.

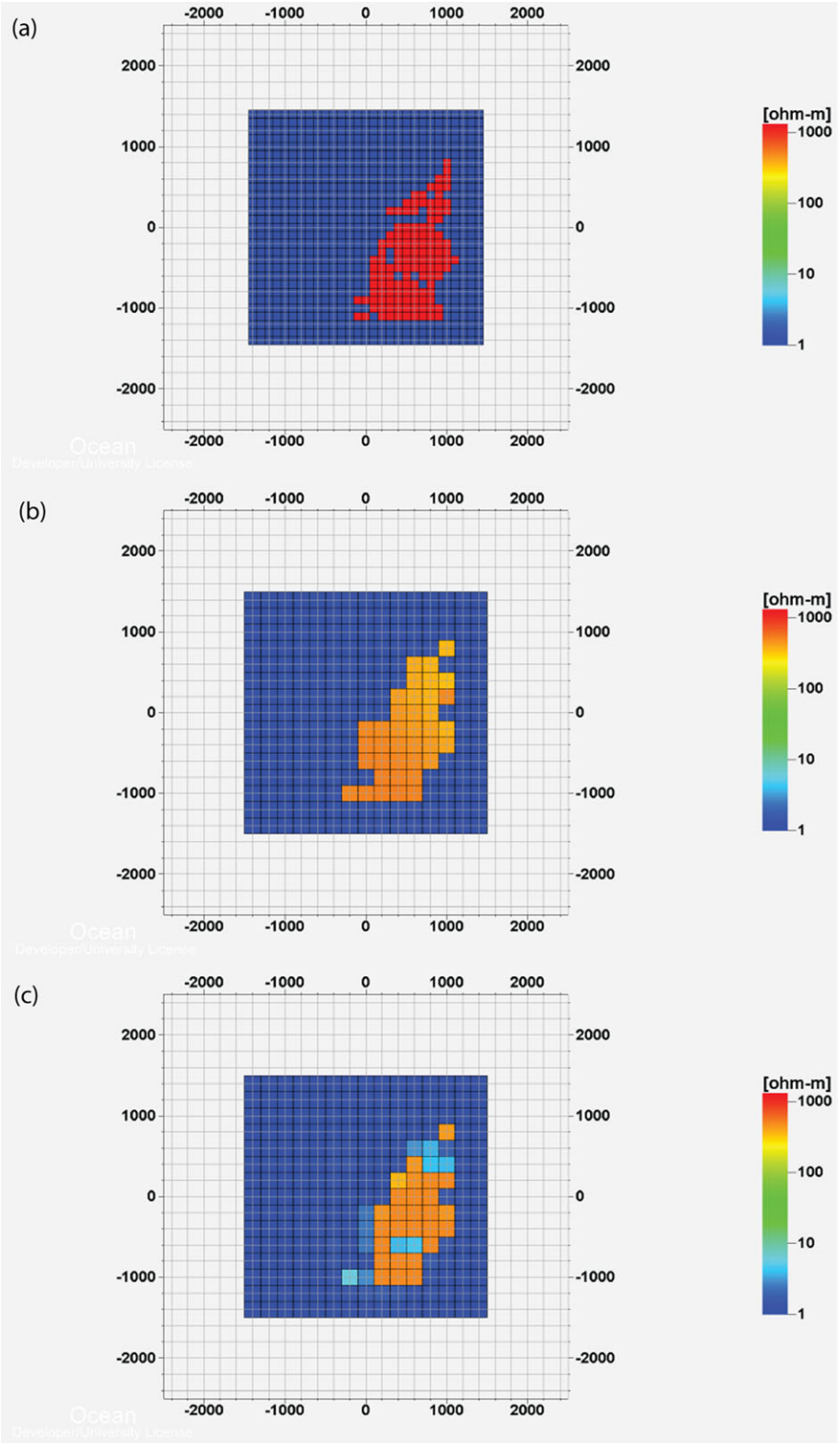

Figure 5 (a) Plan view of the Harding Central reservoir model at 1600 m depth. (b) Plan view of the Harding Central reservoir model recovered from 3D inversion of towed streamer EM data at 1600 m depth. (c) Plan view of the Harding Central reservoir model recovered from 3D inversion of conventional marine CSEM data at 1600 m depth.

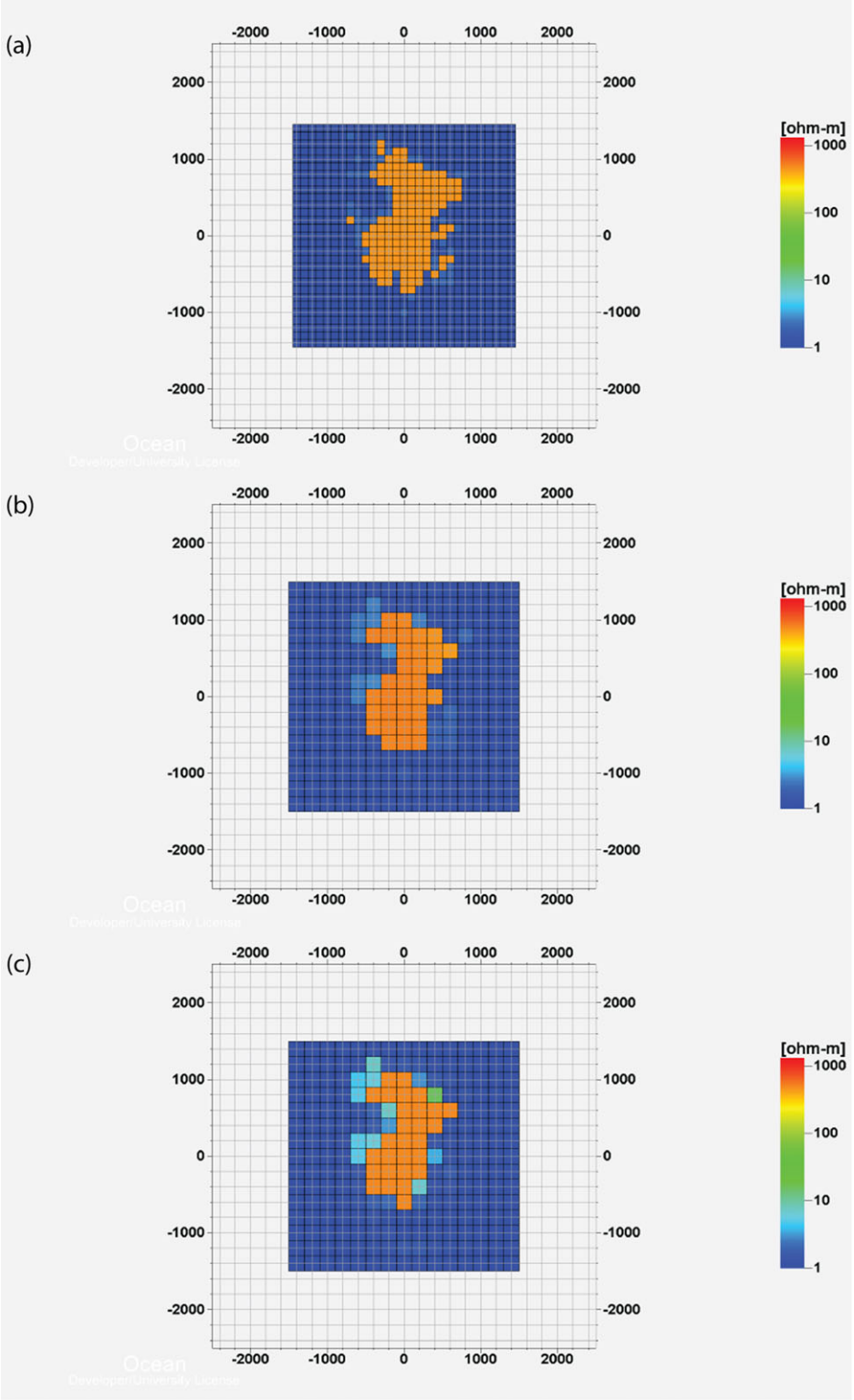

Figure 6 (a) Plan view of the Harding Central reservoir model at 1700 m depth. (b) Plan view of the Harding Central reservoir model recovered from 3D inversion of towed streamer EM data at 1700 m depth. (c) Plan view of the Harding Central reservoir model recovered from 3D inversion of conventional marine CSEM data at 1700 m depth.

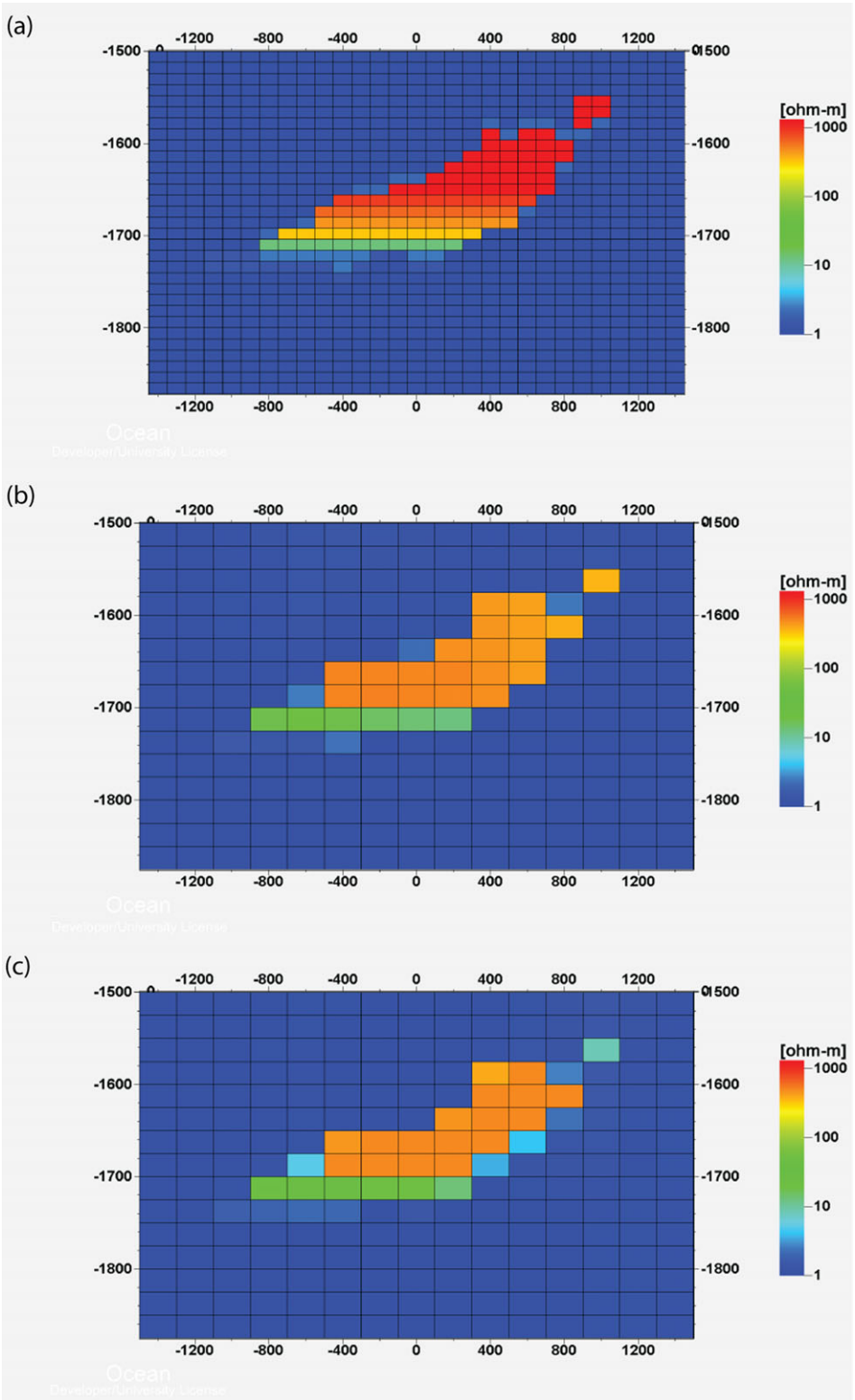

Figure 7 (a) Vertical cross-section of the Harding Central reservoir model along Y = 0 m. (b) Vertical cross-section of the Harding Central reservoir model recovered from 3D inversion of towed streamer EM data along Y = 0 m. (c) Vertical cross-section of the Harding Central reservoir model recovered from 3D inversion of conventional marine CSEM data along Y = 0 m.

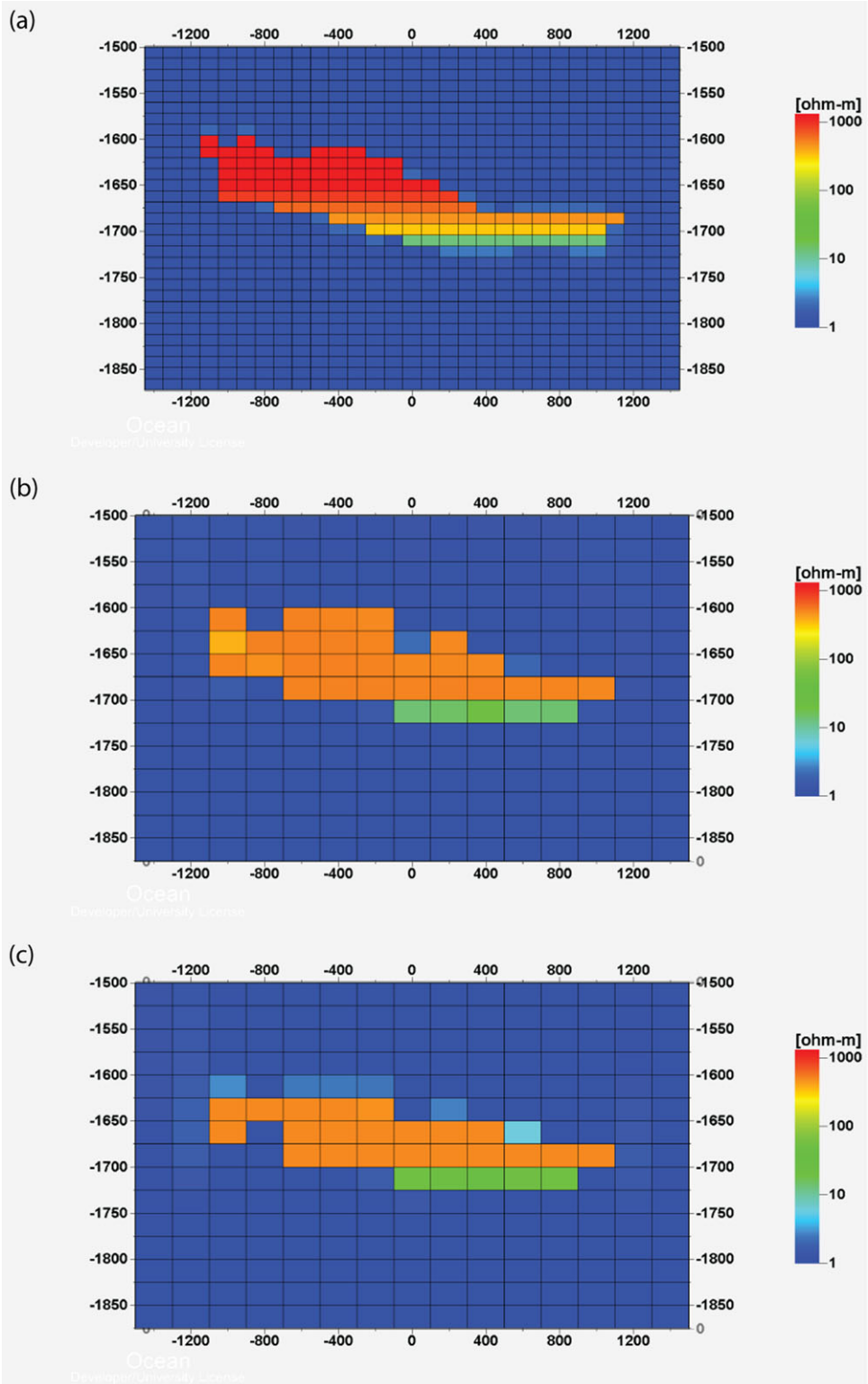

Figure 8 (a) Vertical cross-section of the Harding Central reservoir model along X = 0 m. (b) Vertical cross-section of the Harding Central reservoir model recovered from 3D inversion of towed streamer EM data along X = 0 m. (c) Vertical cross-section of the Harding Central reservoir model recovered from 3D inversion of conventional marine CSEM data along X = 0 m.

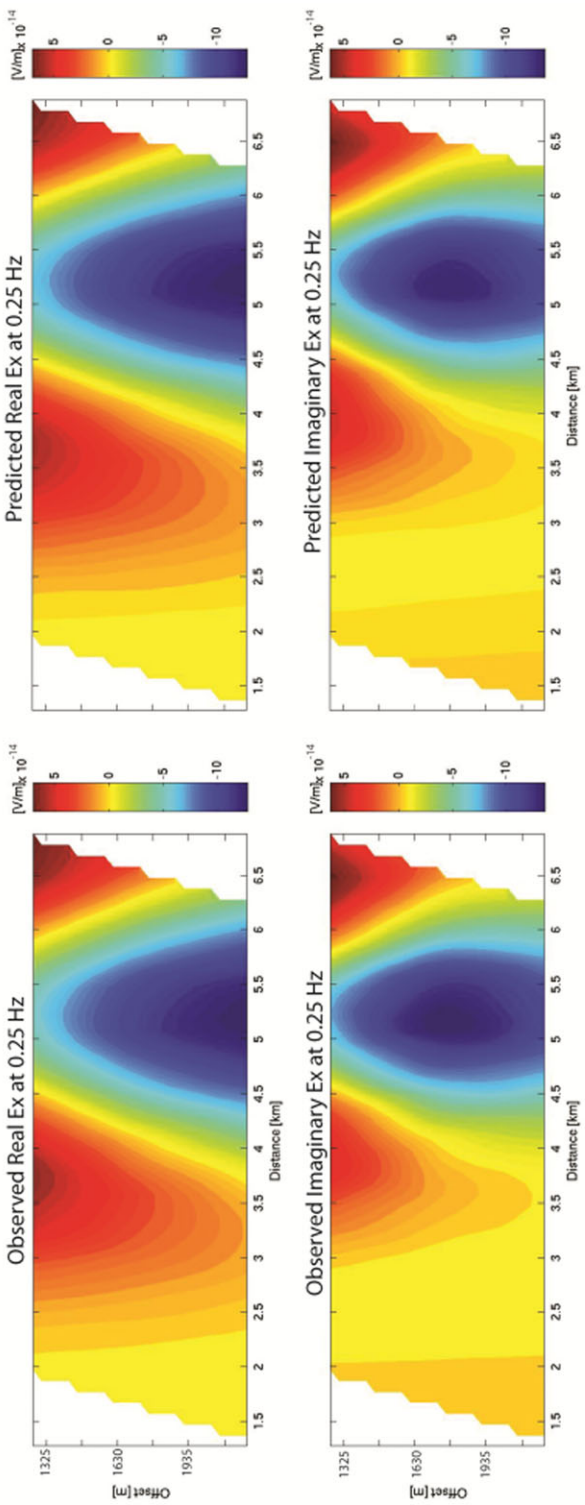

Figure 9 Observed (left panels) and predicted (right panels) real (upper panels) and imaginary (lower panels) data for the in-line electric fields at 0.25 Hz along line 3 from the Harding model study presented as a CMP.

oil- and gasfield covering approximately 20 km^2 that is located in block 9/23B in the UK sector of the North Sea, about 320 km north-east of Aberdeen. The field has a high net-to-gross, high quality, Eocene Balder sandstone reservoir about 1700 m below the seafloor in a 110 m water column. With 300 Mboe initially in place, production commenced in 1996 from the Harding Central and South reservoirs. Since then, two further reservoirs have been developed: Harding South East and by extended reach drilling, Harding North. The reservoirs contain gas and this has been injected back into a gas cap for later production. Oil production is now in decline, with current production of approximately 10 000 bpd with increasing water cut. The remaining hydrocarbon column consists in a gas cap about 100 m thick and a thin oil rim about 20 m thick (Ziolkowski *et al.* 2010).

The Harding Central dynamic reservoir models are populated by porosity and fluid saturations. Core analysis shows the Balder sands at Harding to be clean, so Archie's law is appropriate to relate the petrophysical properties to resistivity. Resistivity logs from well 9/23B-7 showed resistivities greater than 1200 ohm-m through dry gas intervals. In actuality, some intervals may exceed resistivities of 1200 ohm-m but resistive limits of MCSEM responses mean that their values are indiscernible from CSEM data. As per Ziolkowski *et al.* (2010), the 3D model consisted in a 110 m 0.3 ohm-m water column overlying an otherwise homogeneous half-space of 1.0 ohm-m in which the Harding reservoir model was embedded (Fig. 4 a).

The towed EM survey consisted in six survey lines; three oriented north-south and three oriented east-west. The line spacing was 1 km. Each line contained 44 transmitter-receiver pairs (264 total) spaced 500 m apart. The towed EM system consisted in a 300 m long electric bipole transmitter towed 10 m below the sea-surface and in-line electric field receivers towed 50 m below the sea-surface at offsets of 1325 m 1850 m, 2025 m and 2545 m. Data were simulated for 010, 0.25 and 1.00 Hz and contaminated with 2% random Gaussian noise. The inversion was run until the normalized misfit calculated as the L2 norm of the residuals divided by the L2 norm of the observed data reached 2%.

The MCSEM survey consisted in six survey lines, three oriented north-south and three oriented east-west. The MCSEM survey was actually collocated with the towed EM survey. The line spacing was 1 km. Each line contained 11 receivers spaced 500 m apart, giving a total of 66 receivers. Data were simulated to offsets of 5500 m for in-line and vertical electric fields and transverse magnetic fields at frequencies of 0.10, 0.25, 0.50 and 0.75 Hz. The synthetic data were also

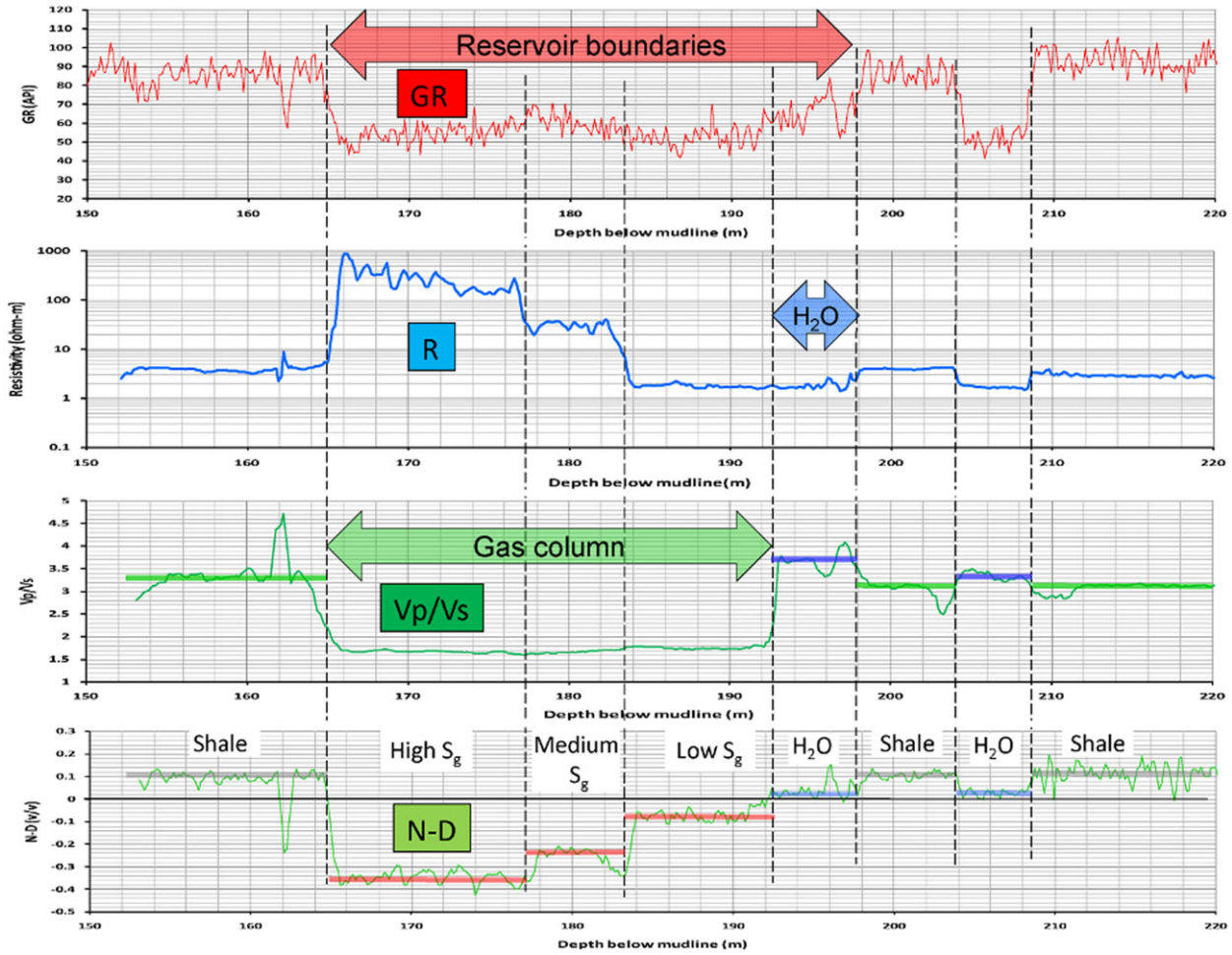

Figure 10 Selected Peon 35/2-1R discovery well logs: Gamma Ray (GR; API); Resistivity (R; ohm-m); Vp/Vs (dimensionless); Neutron porosity – density (N-D; dimensionless). The depth (m) is relative to the seafloor. (Courtesy of PGS.)

contaminated by 2% random Gaussian noise. The inversion was run until the normalized misfit calculated as the L2 norm of the residuals divided by the L2 norm of the observed data reached 2%.

For 3D inversion of both towed EM and MCSEM data, a common 3D earth model was used. That model consisted in a 110 m thick 0.3 ohm-m water column overlying an otherwise homogeneous half-space of 1.0 ohm-m. The 3D inversion domain was discretized to cells of 200 m x 200 m x 20 m dimension. For the towed streamer EM inversion, a moving sensitivity domain of 8 km x 5 km x 2 km was used. We assumed that the *a priori* model was provided by seismic or other geophysical/geological data. We put a slightly resistive (5 ohm-m) layer at a depth from 1550–1750 m inside the inversion domain for 3D inversion of both towed EM and MCSEM data. These inversions were regularized using the minimum vertical support stabilizer. The inversion required several hours on a single cluster node using two 2.6 GHz Xeon Westmere processors running 6 OpenMP threads each. The results of the 3D towed streamer EM inversion are shown in Fig. 4(b) (with transmitter positions superimposed, in 3D view). The result of the 3D MCSEM inversion are shown in Figure 4(c) (with receiver positions superimposed, in 3D view). Figures 5 and 6 show horizontal sections of the (a) true model, (b) results of the 3D towed streamer EM inversion and (c) results of the 3D MCSEM inversion at the depths of 1600 and 1700 m. Figures 7 and 8 show vertical cross-sections of the (a) true model, (b) results of the 3D towed streamer EM inversion and (c) results of the 3D MCSEM inversion, along Y = 0 m and X = 0 m.

As one can see, there is much similarity between the results from the towed EM and MCSEM inversions. For all intents and purposes, the results may be considered equivalent.

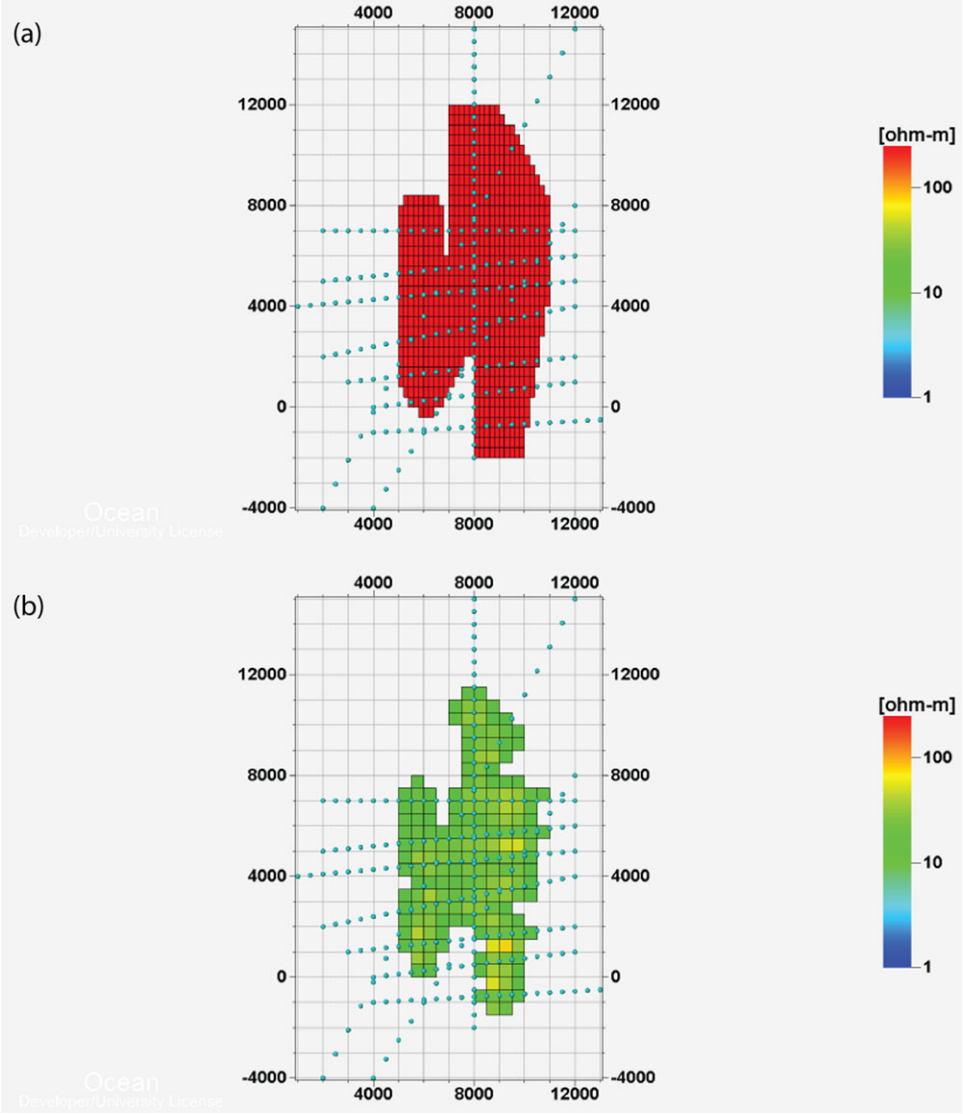

Figure 11 (a) Plan view of the Peon reservoir model at 170 m depth, with resistivity values greater than 10 ohm-m shown. As inferred from well logs, the resistivity at this depth is 280 ohm-m. The blue dots indicate the different transmitter positions of the survey. (b) Plan view of the Peon reservoir model recovered from 3D inversion of towed streamer EM data, with resistivity values greater than 10 ohm-m shown. The blue dots indicate the different transmitter positions of the survey.

Figure 9 shows an example of the 0.25 Hz observed and predicted anomalous data for line 3 (which crosses the Harding reservoir) presented as common midpoint (CMP) plots.

3.2 Peon

In the second model study, we consider a different type of exploration play. Peon is a large shallow gas deposit discovered in 2005 in the Norwegian sector of the North Sea, approximately 100 km west of Florø. The deposit covers approximately 80 km^2 and has a high net-to-gross, high quality, unconsolidated homogeneous sandstone reservoir about 165 m below the seafloor in a 384 m water column. There are no visible signs of gas migration to the seafloor, and there are no signs of gas hydrates in the area, presumably because the water depth is too shallow for gas hydrates to be stable. With 35 GSm^3 gas in place, production is planned to commence in 2014 (Erichsen 2009). Shallow gas deposits such as Peon have never been commercially developed in the North Sea. However, such unconventional deposits exist in the North Sea and

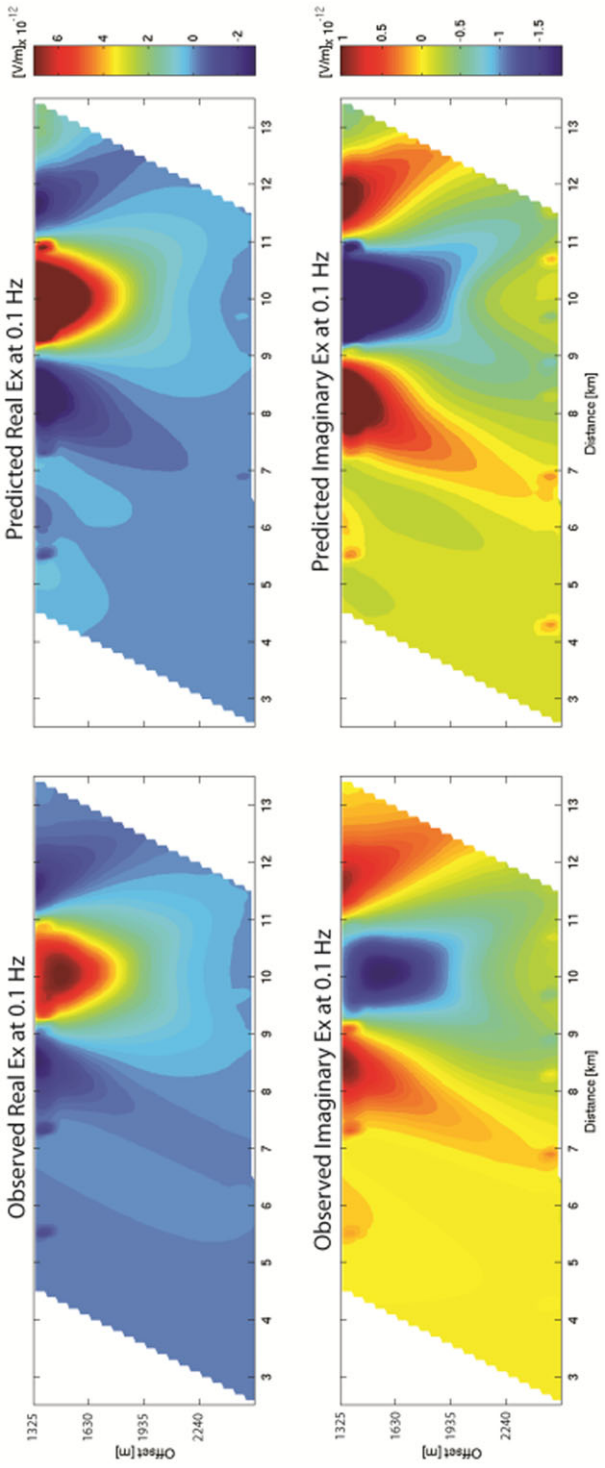

Figure 12 Observed (left panels) and predicted (right panels) real (upper panels) and imaginary (lower panels) data for the in-line electric fields at 0.1 Hz along line 6 from the Peon model study presented as a CMP.

other hydrocarbon proficient basins and they represent a new infrastructure-led exploration strategy for mature basins.

The logs of discovery well 35/2-1R have been analysed to better understand the Peon reservoir architecture. The total thickness of the reservoir interval, as indicated by a gamma ray log (Fig. 10, GR, red), is about 33 m but the Vp/Vs ratio (Fig. 10, Vp-Vs, green) shows that the gas column is about 28 m thick. The neutron porosity-density log (Fig. 10, N-D, black) shows there are three levels of gas saturation in the column (95%, 80% and 10%) but only the high and medium saturation intervals have an appreciable resistivity signature (Fig. 10, R, blue). The resistivity model of the hydrocarbon-charged interval can be described by two consecutive layers; the upper layer being 12 m thick with a resistivity of 280 ohm-m and the lower layer 6 m thick with a resistivity of 30 ohm-m. A horizontal cross-section at 170 m depth is shown in Fig. 11(a).

The towed EM survey consisted in 10 survey lines of arbitrary orientation (Fig. 11). The towed EM system consisted in a 300 m long electric bipole transmitter towed 10 m below the sea-surface and in-line electric field receivers towed 100 m below the sea-surface at offsets of 1325 m, 1850 m, 2025 m and 2545 m. The earth model consisted in a 384 m thick 0.3 ohm-m water column overlying an otherwise homogeneous half-space of 3.0 ohm-m. Data were simulated for 0.10, 0.25 and 1.00 Hz and were contaminated with 2% random Gaussian noise. The inversion was run until the normalized misfit calculated as the L2 norm of the residuals divided by the L2 norm of the observed data reached 2%. A moving sensitivity domain of 8 km x 5 km x 1.5 km was used. The 3D inversion domain was discretized to cells of 500 m x 500 m x 100 m dimension. No *a priori* model was used, the inversion itself was unconstrained and was regularized using the minimum vertical support stabilizer. The inversion required several hours on a single cluster node using two 2.2 GHz Intel Sandybridge processors running eight cores each (2 MPI processes and 8 OpenMP threads each). Results of the 3D towed streamer EM inversion are shown in Fig. 11(b). Figure 12 presents an example of the 0.1 Hz observed and predicted anomalous data for line 6 (which crosses the Peon reservoir) presented as common midpoint (CMP) plots. Similar to Harding, the very high resistivity of the dry gas saturates the EM responses, meaning that the very high resistivities are not recovered. However, the reservoir container is appropriately recovered. In a practical situation, this would be sufficient to provide an initial estimate of Peon's volumetrics and to warrant further, more detailed analysis.

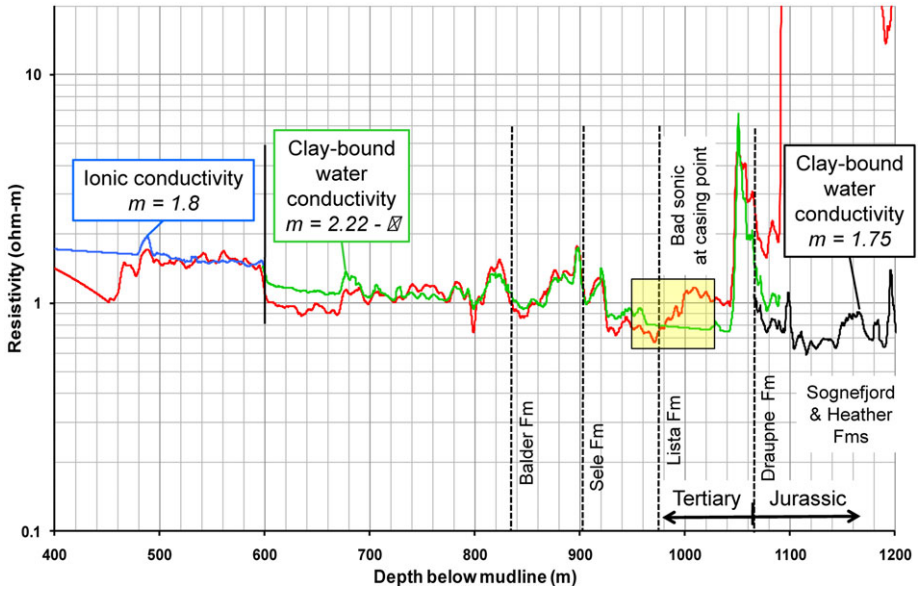

Figure 13 Interpretation of resistivity logs for TWGP well 31-21. The depth is relative to the seafloor. (Courtesy of PGS.)

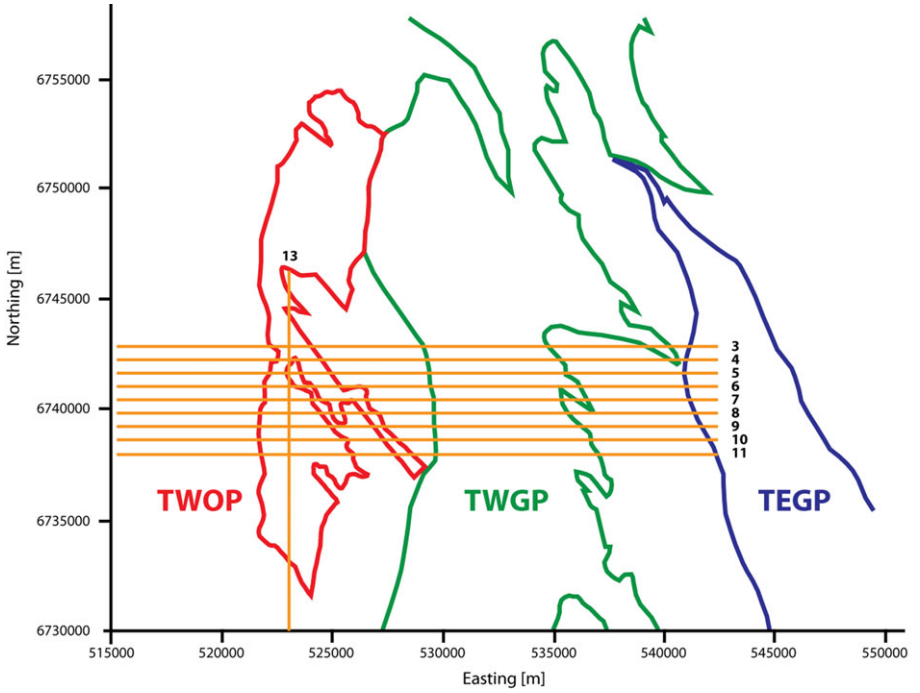

Figure 14 Map of towed streamer EM lines 3–11 used for 3D inversion, with the TEGP, TWGP and TWOP outlines superimposed. In subsequent figures, results from line 6 shall be presented.

4 CASE STUDY – TROLL

The Troll field, operated by Statoil, is located in the Norwegian sector of the North Sea within blocks 31/2, -3, 5 and -6. The field is separated into three parts; the Troll West Oil Province (TWOP), the Troll West Gas Province (TWGP) and the Troll East Gas Province (TEGP). The reservoir intervals are Jurassic (Songefjord Formation) sandstones. Gas-filled reservoir intervals have resistivities of approximately 70 ohm-m, while the water-saturated sands and overburden have resistivities in the range of 0.5–2 ohm-m (Fig. 13). Previous analyses have suggested that the overburden resisitivity is anisotropic

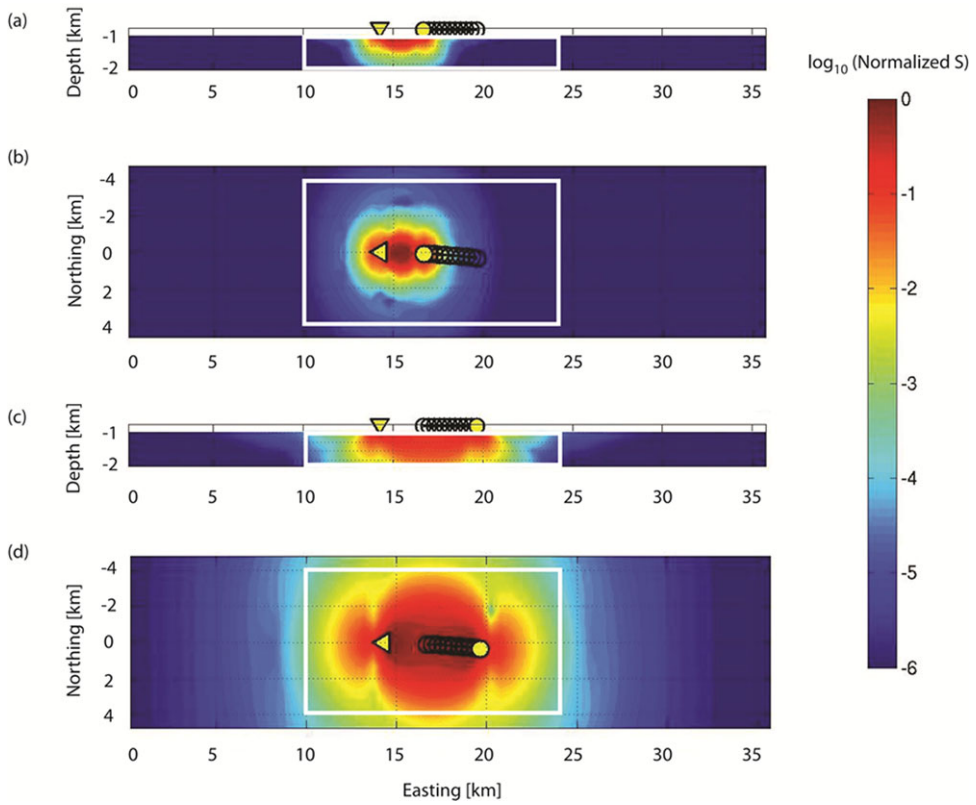

Figure 15 Example of the vertical (panels a and c) and horizontal (panels b and d) dimensions of a sensitivity domain used in the Troll case study. This figure presents the integrated sensitivities for a towed streamer EM system consisting in an 800 m long electric bipole transmitter towed 10 m below the sea-surface and in-line electric field receivers towed 100 m below the sea-surface at offsets between 2400 m for 1.00 Hz (panels a and b) and 5400 m for 0.10 Hz (panels c and d). The earth model consisted in a 320 m thick 0.3 ohm-m water column overlying an otherwise homogeneous, isotropic half-space of 2.0 ohm-m. A sensitivity domain of dimension 14 km x 8 km x 2.0 km (white box) captures over 95% of the integrated sensitivity for the towed streamer EM system for all frequencies and offsets.

though fairly constant: 1.5–1.8 ohm-m for horizontal resistivity and 3.0–3.3 ohm-m for vertical resistivity. However, in the case of in-line dipole-dipole configuration of the towed streamer EM system we can use 3D isotropic inversion as the first approximation. The results of anisotropic inversion will be presented in a separate paper. The TWGP is an ideal CSEM target and has been previously surveyed for various conventional CSEM field trials (e.g., Amundsen, Johansen and Rosten 2004; Gabrielsen *et al.* 2009). A field trial of the towed streamer EM system was undertaken over the Troll field during 2010. The aim of the survey was to demonstrate that the towed streamer EM system was capable of acquiring EM data suitable for delineating the Troll reservoir structures and for extracting subsurface information about them via 3D inversion.

The Troll field trial comprises 12 lines of data (lines 3–11 are shown in Fig. 14) acquired above benign bathymetry at an acquisition speed of 4 knots. In total, 300 line km of data were acquired with the data processed to 250 m CMPs. Each line contained approximately 100 CMPs. During the survey, the weather was uniformly poor, with sea states of 5 and wind speeds between 3–8 on the Beaufort scale. Nine of the lines (numbers 3–11) crossed the TWOP, TWGP and TEGP from west to east. Another line crossed the TWOP from north to south. Another two lines replicated previous CSEM surveys (e.g., Amundsen *et al.* 2004; Gabrielsen *et al.* 2009). The rate of production is typical for seismic acquisition and is several times faster than conventional marine CSEM acquisition. The data were acquired in water depths of approximately 320 m, with the main reservoir at a depth of 1420 m. A range of reservoir thicknesses occur between 40–100 m, with the TWGP being the thickest and TWOP the thinnest. For this survey, 6500 m of streamer was deployed with eleven receiver offsets between 2400–5400 m. The source operated at 800 A (130 kW of total installed power) with 800 m electrode spacing. The transmitter waveform consisted in a

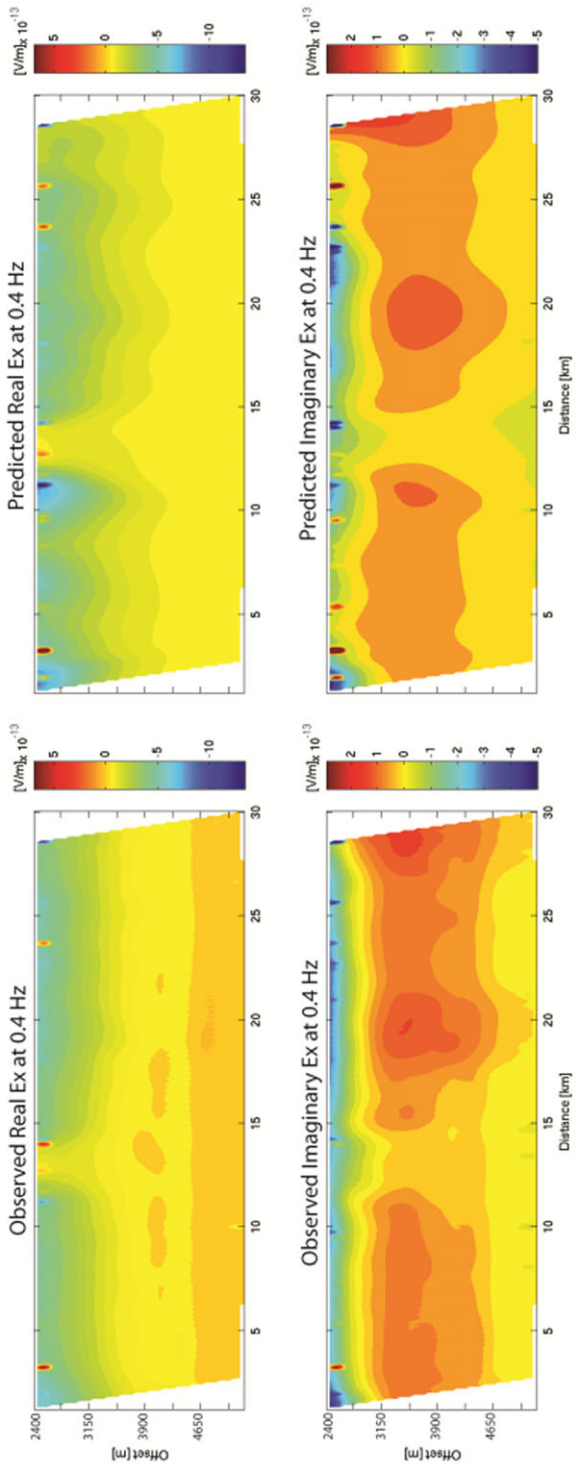

Figure 16 Observed (left panels) and predicted (right panels) real (upper panels) and imaginary (lower panels) data for the in-line electric fields at 0.75 Hz along line 6 from the Troll field trial presented as a CMP.

optimized repeated sequence (ORS) designed to produce two decades of useable frequency content most sensitive to targets in the Troll field. The ORS generated at the source was 100 s long followed by a 20 s silent period. Thus, the total duration of the shot sequence was 120 s. Note that, only in-line electric field data were measured by the towed streamer receivers. The high-data fold was used for noise reduction and led to high-quality data with a sufficiently high signal-to-noise ratio for 1D inversion (Linfoot *et al.* 2011). The final processed data were delivered for 28 frequencies between 0.1–2.75 Hz.

As an example of the sensitivity domain size, we calculated the integrated sensitivities for the towed streamer EM system consisting in a 800 m long electric bipole transmitter towed 10 m below the sea-surface and in-line electric field receivers towed 100 m below the sea-surface at offsets of 2400 m and 5400 m at 0.10 and 1.00 Hz. The earth model consisted in a 320 m thick 0.3 ohm-m water column overlying an otherwise homogeneous, isotropic half-space of 2.0 ohm-m. While the actual system had intermediate offsets and other frequencies, those cited are representative of both the highest frequency/shortest offset and the lowest frequency/longest offset configurations used in our inversion. As can be seen in Fig. 15, a moving sensitivity domain of dimension 14 km x 8 km x 2 km captures over 95% of the integrated sensitivity for the towed streamer EM system used in the Troll field trial. Note that this sensitivity domain is significantly smaller than the Troll earth model survey, which would be considered a very small survey by commercial operations.

We then applied our 3D inversion to all of the towed streamer EM data at five frequencies logarithmically spaced between 0.1–2.75 Hz. The 3D earth model spanning the entire survey area was discretized to 200 m x 200 m x 50 m cells, from the seafloor at 320 m to a depth of 2320 m. The sediments were assigned a 2 ohm-m isotropic resistivity. The inversion required approximately one day on a single cluster node using two 2.2 GHz Xeon Westmere processors running 6 OpenMP threads each. The L2 norm of the residuals between the observed and predicted EM data, normalized by the L2 norm of the observed data, converged to about 2%. Figure 11(a) illustrates the convergence of the weighted misfit as a function of the inversion iteration. Note that the convergence has asymptotic behaviour, as expected. This further demonstrates the accuracy of the sensitivity calculations from equation (11). Figure 16 presents an example of the 0.75 Hz observed and predicted data presented as common midpoint plots. The data fits for 0.75 Hz are typical of the other frequencies. Figure 17(a) presents an example of the vertical

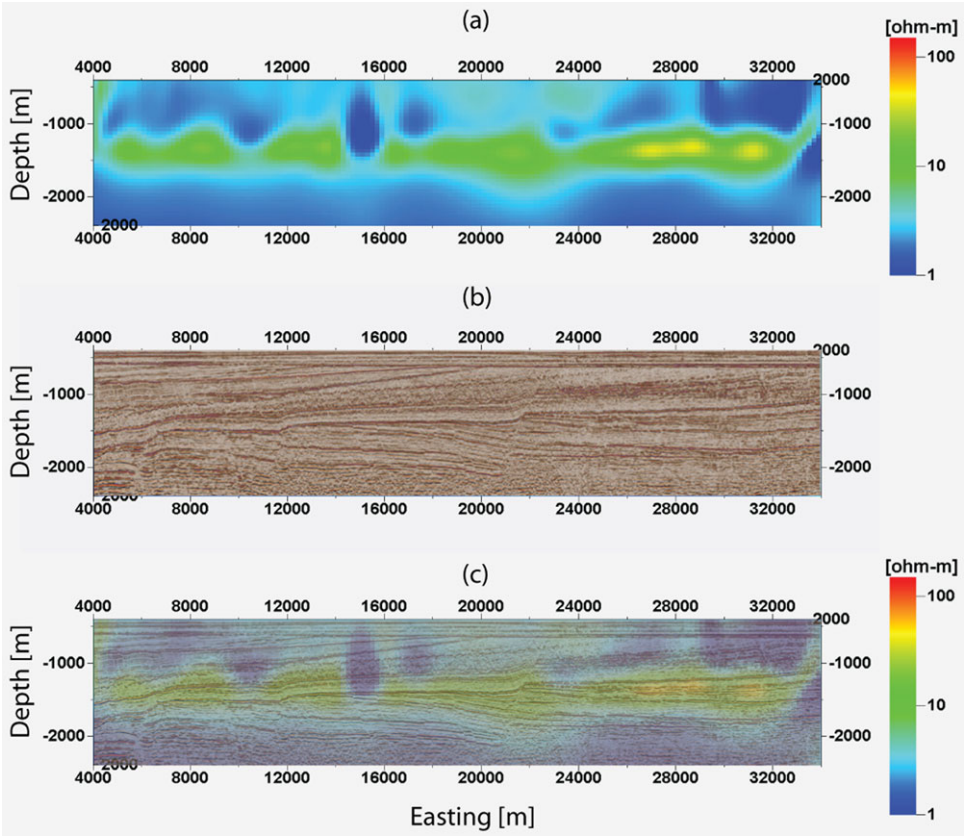

Figure 17 (a) Vertical cross-section along line 6 of the 3D resistivity model as recovered from 3D inversion. (b) Depth converted two-way traveltime seismic image for line 6. (c) Resistivity model corendered with the corresponding seismic image for line 6.

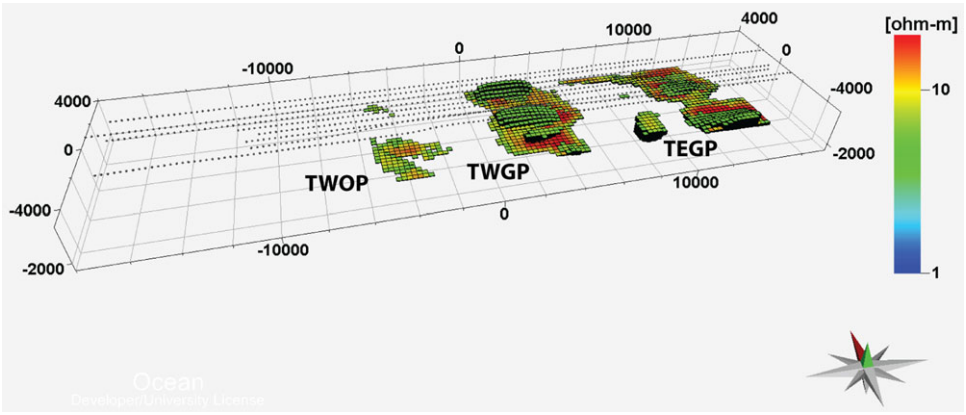

Figure 18 3D perspective view of the Troll reservoir model recovered from 3D inversion of towed streamer EM data, with resistivity values greater than 5 ohm-m shown.

cross-section of the 3D resistivity model along line 6 as recovered from the 3D inversion. Line 6 is oriented east-west and crosses TWOP, TWGP and TEGP, respectively. The results in Fig. 17 are shown for the inversion with minimum vertical support regularization. We should note, however, that, for the current example, no *a priori* information was used. Nevertheless, this figure shows a very promising initial result. The resistive zones are shown in yellow and red in this image and represent the TWGP and TEGP. Line 6 only crosses a very thin part of the TWOP and thus is not readily

apparent in the results. Figure 17(c) presents the same resistivity section with the depth migrated seismic section (Fig. 17 c) superimposed. We note that the resistive targets correspond well with the TWGP and TEGP reservoirs. Given the poor weather conditions during the survey, the robustness of the towed streamer EM system with respect to noise from large wave heights has been demonstrated and shown not to be a factor when inverting the processed EM data. In fact, the inversion was able to converge to about 2% misfit, implying that the towed streamer EM data are of relatively high quality for difficult acquisition conditions.

From the results of the model study on the Harding field, we expect that the use of *a priori* seismic information can improve the resistivity image and indeed enable the towed streamer EM system to acquire seismic data simultaneously with the EM data. We used the *a priori* model estimated from seismic information (Fig. 17b, resistive thin layer with the resistivity of 4 ohm-m between 1450–1550 m inside the inversion domain) and ran the 3D inversion with minimum vertical support regularization. Figure 18 shows a 3D perspective view of the Troll reservoir model recovered from 3D inversion of towed streamer EM data. As expected, one can see clearly the TWOP, TWGP and TEGP as resistive structures, and we consider these results very promising.

5 CONCLUSIONS

A towed streamer electromagnetic (EM) system capable of simultaneous seismic and EM data acquisition has recently been developed and tested in the North Sea. Obviating the need for ocean-bottom receivers, the towed EM system enables EM data to be acquired simultaneously with seismic data over very large areas in frontier and mature basins for higher production rates and relatively lower cost than conventional MCSEM. We introduced a practical methodology for large-scale 3D inversion of towed streamer EM data that is based on a moving sensitivity domain. We demonstrated this with model studies for the Harding and Peon fields in the North Sea. For Harding, we compared our 3D inversion of towed streamer EM data with 3D inversion of conventional MCSEM data and observed similarity between the 3D resistivity models. For Peon, we demonstrated how 3D inversion of towed streamer EM data recovers the shallow gas deposit. Given the prevalence of such unconventional resources in the North Sea and similar basins, this opens up the possibility of infrastructure-led exploration. We also presented a case study for the 3D inversion of towed streamer EM data from a 2010 field trial over the Troll field in the Norwegian North Sea. We demonstrated the ability of the method to image the Troll West Oil and Gas Provinces and Troll East Gas Province reservoirs from the towed streamer EM survey. Given the poor weather conditions during the field trial, the robustness of the towed streamer EM system with respect to noise from large wave heights was demonstrated and shown not to be a factor when inverting the processed EM data. Indeed, the data of were very high quality and the 3D inversion was able to converge successfully to a 3D resistivity model that correlated well with the depth migrated seismic model. We conclude that 3D inversion of data from the current generation of towed streamer EM systems can adequately recover hydrocarbon-bearing formations to depths of approximately 2 km and that this bodes well for continued future developments of the technology.

ACKNOWLEDGEMENTS

The authors acknowledge TechnoImaging and Petroleum GeoServices for support of this research and permission to publish.

The authors also acknowledge support from the University of Utah's Consortium for Electromagnetic Modeling and Inversion (CEMI) and Center for High Performance Computing (CHPC).

The Harding 3D resistivity models were developed as part of the research project H0531E between PGS, BP and the UK Department of Trade and Industry (now Business, Innovation and Skills). BP and Maersk, as operators of the Harding field, are acknowledged for release of the Harding reservoir model. Drs. Bruce Hobbs and Ed Morris are acknowledged for their assistance with the Harding reservoir models.

Statoil is acknowledged for release of data relating to the Peon discovery and the Troll field trial.

REFERENCES

Amundsen H.E.F., Johansen S. and Rosten T. 2004. A sea bed logging (SBL) calibration survey over the Troll gas field. Presented at 66th *EAGE Conference and Exhibition*, Paris.

Anderson C. and Mattsson J. 2010. An integrated approach to marine electromagnetic surveying using a towed streamer and source. *First Break*, **28**(*5*), 71-75.

Avdeev D.B., Kuvshinov A.V., Pankratov O.V. and Newman G.A. 1997. High-performance three-dimensional electromagnetic modeling using modified Neumann Series: Wide-band numerical solution and examples. *Journal of Geomagnetism and Geoelectricity* **49**, 1519-1539.

Beamish D. 2003. Airborne EM footprints. *Geophysical Prospecting* **51**, 49-60.

Commer M. and Newman G.A. 2008. New advances in controlled source electromagnetic inversion. *Geophysical Journal International* **172**, 513-535.

Constable S. 2010. Ten years of marine CSEM for hydrocarbon exploration. *Geophysics*, **75**, 75A67-75A81.

Cox L.H., Wilson G.A. and Zhdanov M.S. 2010. 3D inversion of airborne electromagnetic data using a moving footprint. *Exploration Geophysics* **41**, 250–259.

Cox L.H., Wilson G.A. and Zhdanov M.S. 2012. 3D inversion of airborne electromagnetic data. *Geophysics* **77**, WB59-WB69.

Cox L.H. and Zhdanov M.S. 2007. Large scale 3D inversion of HEM data using a moving footprint. 77th *Annual International Meeting*, *SEG*, Expanded Abstracts, 467-47.

Čuma M., Wilson G.A. and Zhdanov M.S. 2012. Large-scale 3D inversion of potential field data. *Geophysical Prospecting*.

Endo M., Čuma M. and Zhdanov M.S. 2009. Large-scale electromagnetic modeling for multiple inhomogeneous domains. *Communications in Computational Physics* **6**, 269-289.

Erichsen L. 2009. The Peon Field - Unlocking unconventional reserves in the North Sea. Presented at *SPE Bergen*, Bergen.

Gabrielsen P.T., Brevik I., Mittet R. and Løseth L.O. 2009. Investigating the exploration potential for 3D CSEM using a calibration survey over the Troll field. *First Break*, **27** (6), 67-75.

Gribenko A. and Zhdanov M.S. 2007. Rigorous 3D inversion of marine CSEM data based on the integral equation method. *Geophysics* **72**, WA73-WA84.

Hesthammer J., Stefatos A., Boulaenko M., Fanavoll S. and Danielsen J. 2010. CSEM performance in light of well results. *The Leading Edge* **29**, 34-41.

Hohmann G.W. 1975. Three-dimensional induced polarization and electromagnetic modeling. *Geophysics*, **40**, 309-324.

Hursán G. and Zhdanov M.S. 2002. Contraction integral equation method in three-dimensional electromagnetic modeling. *Radio Science* **37**(6), 1089.

Linfoot J.P., Clarke C., Mattsson J. and Price D. 2011. Modeling and analysis of towed EM data – An example from a North Sea field trial. Pre- sented at the 73rd EAGE Conference and Exhibition, Vienna.

Liu G. and Becker A. 1990. Two-dimensional mapping of sea-ice keels with airborne electromagnetics. *Geophysics* **55**, 239-248.

Mackie R., Watts M.D. and Rodi W. 2007. Joint 3D inversion of CSEM and MT data. 77th *Annual Meeting*, SEG, Expanded Abstracts.

Mattsson J.A., Bjornemo E., McKay A. and Ronaess M. 2012. Towed EM system data - error analysis. Presented at 74th *EAGE Conference and Exhibition*, Copenhagen.

Mattsson J.A., Lund L.L., Lima J.L., Englemark F.E. and McKay A.M. 2010. Case study - A towed EM test at the Peon discovery in the North Sea. Presented at 72nd *EAGE Conference and Exhibition*, Barcelona.

McGillivray P.R., Oldenburg D.W., Ellis R.G. and Habashy T. 1994. Calculation of sensitivities for the frequency-domain electromagnetic problem. *Geophysical Journal International* **114**, 1-4.

McKay A., Clarke C., Linfoot J. and Mattsson J. 2011. Interpretative quality control of towed EM data - Examples from the North Sea. Presented at 73rd *EAGE Conference and Exhibition*, Vienna.

Portniaguine O. and Zhdanov M.S. 1999. Focusing geophysical inversion images. *Geophysics* **64**, 874-887.

Raiche A.P. 1974. An integral equation approach to three-dimensional modelling. *Geophysical Journal of the Royal Astronomical Society* **36**, 363-376.

Reid J.E., Pfaffling A. and Vrbancich J. 2006. Airborne electromagnetic footprints in 1D earths. *Geophysics* **71**, G63-G72.

da Silva N.V., Morgan J.V., MacGregor L. and Warner M. 2012. A finite element multifrontal method for 3D CSEM modeling in the frequency domain. *Geophysics* **77**, E101–E115.

Singer B.S. and Fainberg E.B. 1995. Generalization of the iterative dispersive method for modeling electromagnetic fields in nonuniform media with displacement currents. *Journal of Applied Geophysics* **34** , 41-46.

Støren T., Zach J.J. and Maaø F.A. 2008. Gradient calculations for 3D inversion of CSEM data using a fast finite-difference time-domain modeling code. Presented at 70th *EAGE Conference and Exhibition*, Rome.

Tikhonov A.N. and Arsenin Y.V. 1977. *Solution of Ill-posed Problems* . Winston, New York.

Weidelt P. 1975. EM induction in three-dimensional structures. *Journal of Geophysics*, **49**, 60-74.

Weiss C.J. and Constable S.C. 2006. Mapping thin resistors and hydro- carbons with marine EM methods. Part II – Modeling and analysis in 3D. *Geophysics* **71**, G321–332.

Weitemeyer K. and Constable S. 2010. Mapping shallow geology and gas hydrate with marine CSEM surveys. *First Break* **28**, 97–102.

Ziolkowski A., Parr R., Wright D., Nockles V., Limond C., Morris E. and Linfoot J. 2010. Multi-transient electromagnetic repeatability experiment over the North Sea Harding field. *Geophysical Prospecting* **58** , 1159-1176.

Xiong Z. 1992. Electromagnetic modeling of 3D structures by the method of system iteration using integral equations. *Geophysics*, **57**, 1556-1561.

Zhdanov M.S. 2002. *Geophysical Inverse Theory and Regularization Problems*. Elsevier, Amsterdam.

Zhdanov M.S. 2009. *Geophysical Electromagnetic Theory and Methods*. Elsevier, Amsterdam.

Zhdanov M.S., Gribenko A. and Čuma M. 2008. Regularized focusing inversion of marine CSEM data using minimum vertical support stabilizer. 78th *Annual Meeting*, SEG, Expanded Abstracts.

Zhdanov M.S., Čuma M., Wilson G.A., Velikhov E.P., Black N. and Gribenko A. 2011. Iterative electromagnetic migration for 3D inversion of marine CSEM data. *Geophysical Prospecting* **59**, 1101-1113.